

# Adaptive Frequency Enhancement Network for Single Image Deraining

Fei Yan<sup>\*1</sup>, Yuhong He<sup>\*2</sup>, Keyu Chen<sup>†1</sup>, En Cheng<sup>1</sup> and Jikang Ma<sup>1</sup>

**Abstract**—Image deraining aims to improve the visibility of images damaged by rainy conditions, targeting the removal of degradation elements such as rain streaks, raindrops, and rain accumulation. While numerous single image deraining methods have shown promising results in image enhancement within the spatial domain, real-world rain degradation often causes uneven damage across an image’s entire frequency spectrum, posing challenges for these methods in enhancing different frequency components. In this paper, we introduce a novel end-to-end Adaptive Frequency Enhancement Network (AFENet) specifically for single image deraining that adaptively enhances images across various frequencies. We employ convolutions of different scales to adaptively decompose image frequency bands, introduce a feature enhancement module to boost the features of different frequency components and present a novel interaction module for interchanging and merging information from various frequency branches. Simultaneously, we propose a feature aggregation module that efficiently and adaptively fuses features from different frequency bands, facilitating enhancements across the entire frequency spectrum. This approach empowers the deraining network to eliminate diverse and complex rainy patterns and to reconstruct image details accurately. Extensive experiments on both real and synthetic scenes demonstrate that our method not only achieves visually appealing enhancement results but also surpasses existing methods in performance. The source code is available at <https://github.com/yanfeifei/AFENet>.

## I. INTRODUCTION

Single image deraining focuses on reconstructing a rain-free image from a degraded rainy image captured in rainy conditions, as shown in Fig. 1. Since both the clear image and the nature of rain degradation are typically unknown, image deraining presents as an ill-posed and challenging problem [1]. Rain degradation significantly hinders computer vision tasks such as image classification, object detection, and semantic segmentation [2], [3]. For example, vision-based intelligent driving systems are severely affected in rainy conditions, making it imperative to remove rain and reconstruct high-quality, rain-free images effectively. Traditional methods often rely on mathematical statistics to derive diverse priors by exploring the physical characteristics of rain streaks and accumulation. Various priors, including layer priors with the Gaussian mixture model (GMM) [4], discriminative sparse coding (DSC) [5], and high-frequency priors [6], have been proposed to regularize and separate rain streaks. However, these traditional approaches struggle with complex rainy scenes in real-world scenarios.

This work is supported in part by the National Natural Science Foundation of China (62271425 and 62071402). <sup>\*</sup>equal contribution. <sup>†</sup>Corresponding author.

<sup>1</sup>School of Informatics, Xiamen University, Xiamen, China

<sup>2</sup>School of Computer Science and Engineering, Northeastern University, Shenyang, China

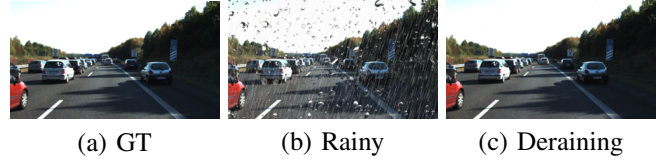


Fig. 1. Example of rain removal in rainy conditions.

In recent times, numerous deep learning-based methods have been developed to learn the transformation from a rainy to a clear image in a data-driven manner [7]–[15]. These methods have significantly advanced the removal of rain streaks and image enhancement in the spatial domain. Yet, the distribution of rain artifacts varies across different frequency ranges, posing a challenge to these methods in effectively enhancing different frequency components within the spatial domain. In real-world rainy scenarios, rain streaks, raindrops, and rain accumulation coexist [1], [16], with rain streaks predominantly present in high-frequency image areas, whereas rain accumulation and raindrops are more prevalent in mid and low frequencies.

To elucidate this, we conduct a frequency analysis in various rainy scenes, analyzing over 1000 pairs of rainy and derained images including conditions with rain streaks, raindrops, and rain accumulation. We utilized the Discrete Cosine Transform (DCT) to separate the frequencies into high, middle, and low bands, calculating the frequency energy and energy error between paired rainy and clean images across different frequencies. As illustrated in Fig. 2, there are notable energy discrepancies at different frequencies. This significant variance in errors across frequency bands highlights the need for targeted enhancement in each band. Moreover, since rain streaks and background details are often intertwined in the spatial domain, existing methods struggle to completely eliminate rain streaks and recover structural information in complex rainy scenarios [1], [16], [17]. Most previous works have focused predominantly on spatial information, overlooking distinct frequency information. The differences between rainy and clear image pairs are more distinctly defined in the frequency domain. Consequently, a novel image deraining network that can adaptively enhance the frequency becomes essential for achieving high-quality image reconstruction.

To fulfill this objective, we introduce a novel Adaptive Frequency Enhancement Network (AFENet) for single image deraining, specifically designed to enhance features across different frequency components. Our approach begins with the use of scale-variable convolutions to decompose the image into three distinct frequency components. We

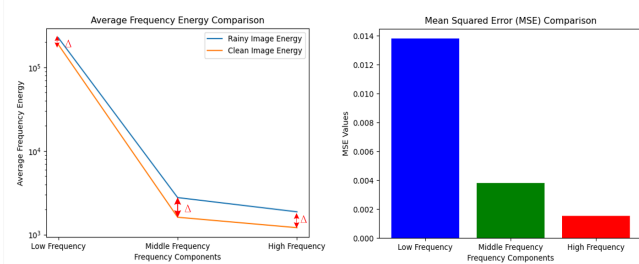


Fig. 2. Frequency Analysis of Various Rainy Images (including rain streaks, raindrops, and rain accumulation) and Clean Images: The left side of the analysis highlights the differences in energy distribution among various frequency components. On the right side, the focus is on the variations in Mean Squared Error (MSE) between rainy and clean images across various frequencies. Here,  $\Delta$  signifies the absolute difference in rainy degradation across these different frequency components.

then present a novel Feature Enhancement Module (FEM), which effectively segments and manages information within different frequency domain branches, thereby enhancing features across these components. Subsequently, we propose an innovative Feature Aggregation Module (FAM) that facilitates the interactive fusion of features from various frequency branches. This comprehensive enhancement across all frequency components enables the deraining network to effectively remove a wide array of complex rainy patterns and reconstruct image details. Extensive testing on both real and synthetic scenes has shown that our method not only achieves visually appealing results but also surpasses existing methods in effectiveness.

In summary, the key contributions of our research are as follows:

- We introduce the Adaptive Frequency Enhancement Network (AFENet), a novel approach designed to effectively enhance features in different frequency components, thus aiding in reconstructing high-quality, clean images.
- A novel Frequency Enhancement Module and Feature Aggregation Module are developed, aiming at proficient feature enhancement and fusion across various frequency branches.
- Through comprehensive experiments, we demonstrate that our method not only achieves aesthetically pleasing enhancement results but also consistently outperforms existing techniques in both real and synthetic scenes.

## II. RELATED WORK

Over the past decade, significant advancements have been achieved in the field of image restoration under adverse weather conditions [13], [18]–[21], [21]–[31], with significant advancements in single image deraining methods garnering widespread attention and achieving notable success [7], [10]–[12], [32]. Current single image deraining techniques can be broadly classified into traditional and deep learning-based methods. Traditional methods focus on the statistical analysis of rain streaks and background scenes, while deep learning-based methods leverage data-driven approaches that

utilize deep neural networks to autonomously extract hierarchical features and develop more sophisticated models to restore rainy images into clean ones.

### A. Traditional Single Image Deraining

Traditional deraining approaches often involve utilizing diverse priors to create additional constraints, forming a cost function, and optimizing it. Luo *et al.* [33] proposed a single-image deraining algorithm based on a non-linear generative model, using dictionary learning and discriminative codes to represent rain layers sparsely. Li *et al.* [4] tackled rain streak removal as a layer decomposition problem, employing Gaussian mixture models as a layer prior. Zhu *et al.* [5] decomposed rainy images into a rain-free background and a rain-streak layer. These methods, while effective on synthetic datasets, often face challenges in real-world scenarios due to mixed and non-uniform degradations and the lack of sufficient paired data for training.

### B. Deep Learning-based Single Image Deraining

Recently, numerous deep learning methods have emerged, demonstrating exceptional performance [5], [30], [31], [34]–[39]. Yang *et al.* [40] developed a network for joint rain detection and removal, handling heavy rain and accumulation. Fu *et al.* [41] introduced a deep detail network for rain streak removal, focusing on high-frequency details. Zhang *et al.* [42] designed a multi-stream dense network for density-aware rain streak removal. Jiang *et al.* [38] proposed a multi-scale progressive fusion strategy to capture global textures of rain streaks. In [39], a multi-stage architecture was introduced for contextualized feature learning. Ye *et al.* [43] employed a bidirectional disentangled translation network for joint rain generation and removal. Xiao *et al.* [44] proposed a Transformer-based image de-raining architecture. Chen *et al.* [8] introduced a Sparse Sampling Transformer for adaptive degradation sampling. Although these methods perform well in spatial domain detail reconstruction, they face challenges in fully restoring images in all frequency bands under complex, real-world rainy conditions, resulting in rain residual and detail distortion in complex and real-world rainy conditions.

## III. PROPOSED METHOD

In this section, we present an in-depth introduction to the newly proposed Adaptive Frequency Enhancement Network (AFENet). The comprehensive architecture of AFENet is illustrated in Fig. 3. AFENet is fundamentally composed of three key components: the Frequency Decomposition Module (FDM), the Frequency Enhancement Module (FEM), and the Frequency Aggregation Module (FAM).

### A. Frequency Decomposition Module

To further elaborate on the innovative design of the Frequency Decomposition Module (FDM), as depicted in Fig. 3(b), we have developed it with the aim of achieving an exhaustive representation across all frequency bands. FDM ingeniously segments rainy images into three distinct

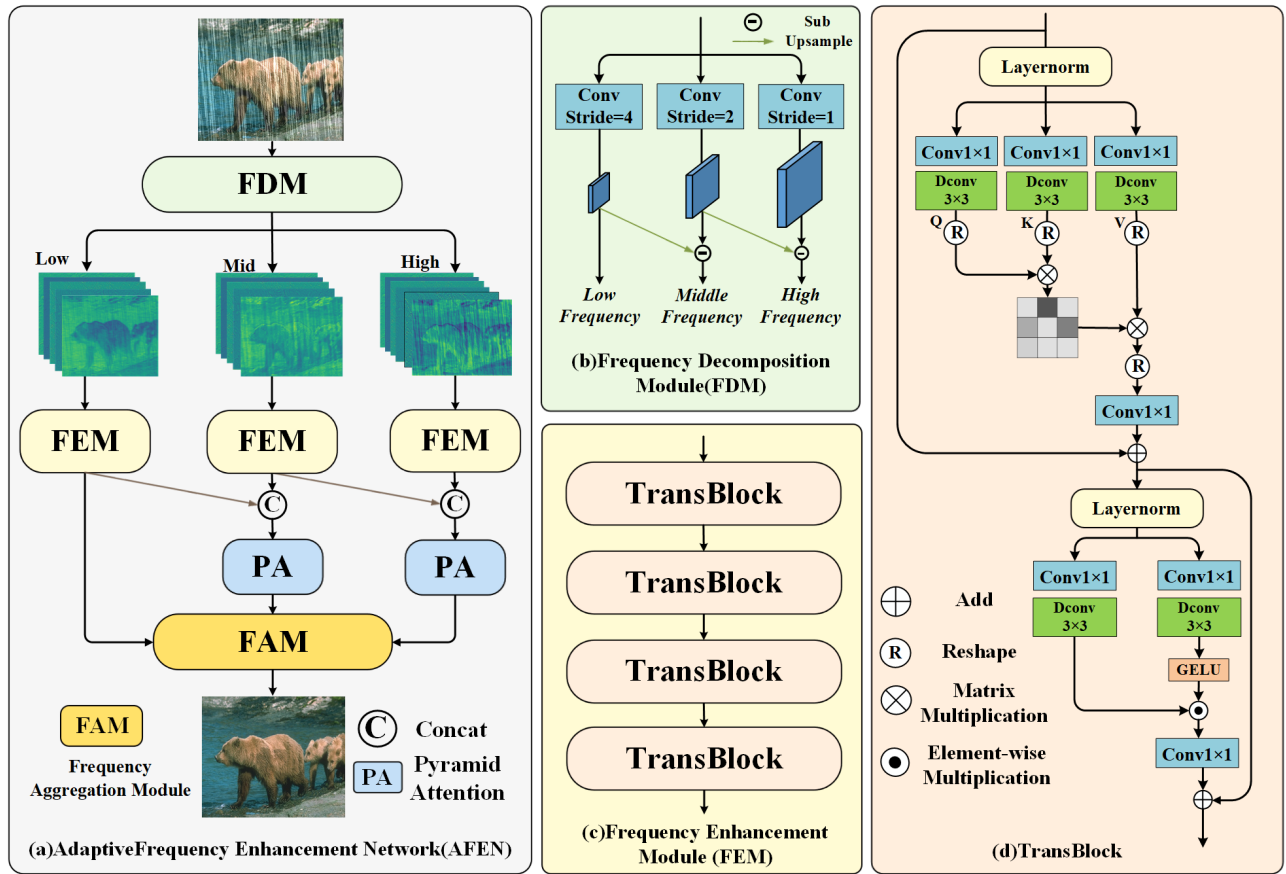


Fig. 3. The architecture of our proposed Adaptive Frequency Enhancement Network (AFENet) includes three key modules: the Frequency Decomposition Module (FDM), which employs a multi-branch architecture to decompose the rainy image content in the frequency domain, thereby enhancing texture details across all frequency components; the Frequency Enhancement Module (FEM), designed to improve the feature representation capabilities; and the Frequency Aggregation Module (FAM), which aggregates the enhanced frequency components from various scales of the rainy image.

frequency bands: high, middle, and low. Diverging from conventional image processing methods like the Discrete Cosine Transform (DCT) [45] or the wavelet transform [46], our approach opts for convolutions with varied receptive fields to adaptively discern features across different frequency ranges. This choice is driven by a critical insight: traditional methods, while precise, often lead to a loss of essential information imperative for low-level restoration tasks due to their deterministic mathematical framework and limited applicability to specific tasks. This is further examined in our ablation studies detailed in Section IV-G. The unique stratification afforded by FDM paves the way for creating specialized frequency-enhancement branches, each tailored to learn representations pertinent to their designated frequency band.

Furthermore, to safeguard pivotal details, we have integrated a novel implicit downsampling method for decomposing frequency-specific features. In this nuanced approach, we utilize convolutional layers with incrementally larger strides for extracting low-frequency features, effectively isolating the high-frequency elements by eliminating lower-frequency components from the initial features. This process entails employing a convolutional layer with a stride of 4 for

the extraction of the low-frequency component, denoted as  $f_l$ . The mid-frequency component  $f_m$  is then isolated by subtracting  $f_l$  from the original features, correspondingly downsampled with a stride of 2. In a similar way, the high-frequency component  $f_h$  is derived by subtracting the features downsampled with a stride of 2 from the original rainy image’s unsampled features, thereby preserving the original spatial dimensions. The formulation of FDM is as follows:

$$\begin{aligned} f_l &= \text{Conv} \downarrow_2 (\text{Conv} \downarrow_2 (I)), \\ f_m &= \text{Conv} \downarrow_2 (I) - \text{Conv} \downarrow_2 (\text{Conv} \downarrow_2 (I)) \uparrow_2, \\ f_h &= \text{Conv}(I) - \text{Conv} \downarrow_2 (I) \uparrow_2, \end{aligned} \quad (1)$$

$\text{Conv} \downarrow_2$  represents the convolution layer with a stride of 2, and  $\text{Conv}$  signifies a convolution layer without downsampling.  $\uparrow_2$  denotes the bilinear upsampling operation. This frequency decomposition approach offers two primary benefits. Firstly, unlike traditional multi-branch networks, it improves network efficiency by reducing feature resolution. Secondly, it boosts performance by embracing multi-scale representation learning, thereby effectively tackling degradations across different frequencies [47].

## B. Frequency Enhancement Module

Continuing from the previous explanation, the real-world application of image deraining, as demonstrated in Fig. 2, clearly highlights the necessity of addressing a full-spectrum degradation problem. It becomes imperative to enhance features across the entire frequency spectrum to effectively tackle this issue. Therefore, in our proposed architecture, as shown in Fig. 3(c), the Frequency Enhancement Module (FEM) is utilized to augment each set of features corresponding to high, mid, and low frequencies.

Recognizing that rainy images often suffer from global degradation, our Feature Extraction Module (FEM) is specifically designed to extract both global and local features, an approach that addresses the complex nature of image de-raining. The FEM employs an innovative transformer block named the Multi-Dconv Head Transposed Attention (MDTA), which marks a significant advancement over traditional CNNs. The core strength of the MDTA lies in its ability to handle global features more effectively than CNNs, primarily due to the transformer architecture’s inherent prowess in this aspect.

MDTA stands out by utilizing self-attention (SA) mechanisms across channels as opposed to spatial dimensions, enabling the computation of cross-covariance. This results in the generation of an attention map that implicitly captures the global context of the image. A key feature of MDTA is the integration of depth-wise convolutions that focus on the local context. These convolutions precede the computation of feature covariance, which is crucial for constructing the global attention map. The depth-wise convolutions thus ensure a balanced focus on both local and global aspects of the image features, enhancing the module’s effectiveness in de-raining applications. The operational mechanism of MDTA is defined as follows:

$$\begin{aligned} \hat{X} &= W_p \text{Attention}(\hat{Q}, \hat{K}, \hat{V}) + X \\ \text{Attention}(\hat{Q}, \hat{K}, \hat{V}) &= \hat{V} \cdot \text{Softmax}(\hat{K} \cdot \hat{Q} / \alpha) \end{aligned} \quad (2)$$

where  $X$  and  $\hat{X}$  are the input and output feature maps.  $\hat{Q} \in R^{\hat{H}\hat{W}\times\hat{C}}$ ;  $\hat{K} \in R^{\hat{C}\times\hat{H}\hat{W}}$ ,  $X \in R^{\hat{H}\times\hat{W}\times\hat{C}}$  and  $\hat{V} \in R^{\hat{H}\hat{W}\times\hat{C}}$  matrices are obtained after reshaping tensors from the original size  $R^{\hat{H}\times\hat{W}\times\hat{C}}$ . Here,  $\alpha$  is a learnable scaling parameter to adjust the magnitude of the dot product of  $K$  and  $Q$  before applying the softmax function.

Furthermore, to capture local features, the FEM introduces Gated-Dconv Feed-Forward Network (GDFN) [48]. The GDFN captures information flow across different hierarchical levels within our framework. This method enables each level to concentrate on intricate details, complementing other levels and thereby enriching the features with contextual information. GDFN is formulated as:

$$\begin{aligned} \hat{X} &= W_p^0 \text{Gating}(X) + X \\ \text{Gating}(X) &= \phi(W_d^1 W_p^1(\text{LN}(X))) \odot W_d^2 W_p^2(\text{LN}(X)) \end{aligned} \quad (3)$$

where  $\odot$  denotes element-wise multiplication,  $\phi$  represents the GELU non-linearity, and LN is the layer normalization.

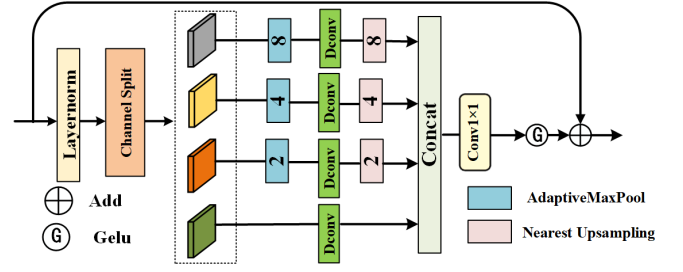


Fig. 4. Frequency Aggregation Module (FAM): a multi-scale feature generation unit to produce features at multiple scales.

enables each branch to selectively fuse the corresponding frequency components at various stages, significantly enhancing the representation capability of each branch.

Moreover, given the inherent challenge of restoring high-frequency feature components, we introduce a strategy to enhance these complex frequency components from coarse to fine. Specifically, we facilitate interaction between different frequency components, progressively leveraging the enhanced lower-frequency representations to enhance the higher-frequency components. This is achieved by concatenating these frequency components together. Subsequently, we employ Pyramid Attention to refine the details in the higher-frequency components further. This strategy not only addresses the difficulty of restoring high-frequency details but also ensures a comprehensive and integrated enhancement across all frequency bands. We define this enhancement and interaction process as follows:

$$\begin{aligned} \hat{F}_l &= \text{enhance}(f_l), \\ \hat{F}_m &= \text{PA}(\text{enhance}(F_m) \odot \text{enhance}(F_l)), \\ \hat{F}_h &= \text{PA}(\text{enhance}(F_h) \odot \text{enhance}(F_m)) \end{aligned} \quad (4)$$

where  $\text{enhance}(\cdot)$  denotes a set of several frequency enhancement modules (FEM), and  $\text{PA}(\cdot)$  denotes Pyramid Attention, which can be found in Fig. 3(a).

## C. Frequency Aggregation Module

In addressing the varied extent of frequency information loss in different areas of rainy images, our method effectively utilizes long-range dependencies derived from multi-scale feature representations. This methodology significantly improves the identification and restoration of crucial features for reconstructing a clean image. This paper provides an in-depth exploration of the Frequency Aggregation Module (FAM), as depicted in Fig. 4. To find an optimal balance between model complexity and the achievement of a pyramid-like feature representation, we initially implemented a channel-wise split operation on the normalized input features. Subsequently, a multi-scale feature generation unit is utilized to produce features at various scales. Specifically, a  $3 \times 3$  depth-wise convolution is applied to the first segment. The remaining segments undergo a series of upsampling and downsampling operations, each followed by a depth-wise convolution.



TABLE I

QUANTITATIVE COMPARISONS WITH EXISTING STATE-OF-THE-ART DERAINING METHODS. AVERAGE REFERS TO THE AVERAGE PERFORMANCE OF THE FIVE BENCHMARK DATASETS. THE **BOLD** AND UNDERLINE REPRESENT THE BEST AND SECOND-BEST PERFORMANCE RESPECTIVELY.

Metrics	Test100		Rain100H		Rain100L		Test1200		Test2800		Average	
	PSNR	SSIM	PSNR	SSIM	PSNR	SSIM	PSNR	SSIM	PSNR	SSIM	PSNR	SSIM
DerainNet [41]	22.77	0.810	14.92	0.592	27.03	0.884	23.38	0.835	24.31	0.861	22.48	0.796
SEMI [49]	22.35	0.788	16.56	0.486	25.03	0.842	26.05	0.822	24.43	0.782	22.88	0.744
DIDMDN [42]	22.56	0.818	17.35	0.524	25.23	0.741	29.95	0.901	28.13	0.867	24.64	0.770
UMRL [35]	24.41	0.829	26.01	0.832	29.18	0.923	30.55	0.910	29.97	0.905	28.02	0.880
RESCAN [36]	25.00	0.835	26.36	0.786	29.80	0.881	30.51	0.882	31.29	0.904	28.59	0.858
SPANet [50]	23.17	0.833	26.54	0.843	32.20	0.951	31.36	0.912	30.05	0.922	28.66	0.892
PReNet [37]	24.81	0.851	26.77	0.858	32.44	0.950	31.36	0.911	31.75	0.916	29.43	0.897
MSPFN [38]	27.50	0.876	28.66	0.860	32.40	0.933	32.39	0.916	32.82	0.930	30.75	0.903
CRDNet [9]	27.72	0.887	28.63	0.872	33.28	0.952	32.44	0.913	33.39	0.935	31.09	0.912
MPRNet [39]	30.27	0.897	30.41	0.890	36.40	0.965	32.91	0.916	33.64	0.938	32.73	0.921
IDLIR [51]	28.33	0.894	29.33	0.886	35.72	0.965	32.06	<u>0.917</u>	32.93	0.936	31.67	0.920
Uformer-B [52]	29.90	0.906	30.31	0.900	36.86	<u>0.972</u>	29.45	0.903	33.53	0.939	32.01	0.924
IDT [44]	29.69	0.905	29.95	<u>0.898</u>	<u>37.01</u>	0.971	31.38	0.908	33.38	0.937	32.28	0.924
Semi-SwinDerain [34]	28.54	0.893	28.79	<u>0.861</u>	34.71	0.957	30.96	0.909	32.68	0.932	31.14	0.910
LDRNet [53]	<b>31.19</b>	<b>0.913</b>	<u>30.60</u>	0.892	36.73	0.967	<u>32.89</u>	<u>0.917</u>	<u>33.67</u>	<u>0.939</u>	<u>33.02</u>	<u>0.926</u>
AFENet(ours)	<u>30.50</u>	<u>0.918</u>	<b>31.22</b>	<b>0.901</b>	<b>37.66</b>	<b>0.978</b>	<b>33.13</b>	<b>0.925</b>	<b>33.82</b>	<b>0.944</b>	<b>33.27</b>	<b>0.933</b>

TABLE II

QUANTITATIVE COMPARISONS WITH EXISTING STATE-OF-THE-ART DERAINING METHODS IN RAINDS DATASETS.

method	RS		RD		RDS	
	PSNR	SSIM	PSNR	SSIM	PSNR	SSIM
GMM [4]	26.66	0.781	23.04	0.793	21.50	0.669
JCAS [54]	26.46	0.786	23.15	0.811	20.91	0.671
DDN [41]	30.41	0.869	27.92	0.885	26.85	0.796
NLEDN [55]	36.24	0.958	34.87	0.957	32.21	0.934
RESCAN [36]	30.99	0.887	29.90	0.907	27.43	0.818
PReNet [37]	36.63	0.968	34.58	0.964	32.21	0.934
UMRL [35]	35.76	0.962	33.59	0.958	31.57	0.929
JORDER-E [56]	33.65	0.925	33.51	0.944	30.05	0.870
Uformer [52]	40.69	0.972	37.08	0.966	34.99	0.954
MSPFN [38]	38.61	0.975	36.93	0.973	34.08	0.947
MPRNet [39]	40.81	0.981	37.03	<u>0.972</u>	34.99	0.956
CCN [57]	39.17	0.981	37.30	<b>0.976</b>	34.79	0.957
NAFnet [58]	40.39	0.972	37.23	0.974	34.99	0.957
DGUNet [59]	41.09	<b>0.983</b>	37.56	<u>0.975</u>	35.34	0.959
AFENet(ours)	<b>43.17</b>	<u>0.981</u>	<b>38.67</b>	0.969	<b>35.78</b>	<b>0.989</b>

To effectively discern and select discriminative features that capture non-local interactions, we utilize adaptive max pooling on the input features to produce multi-scale features. These features are then concatenated using a  $1 \times 1$  convolution coupled with GELU non-linearity. This process facilitates the integration of both local and global feature relationships. Ultimately, we enhance the output by adding the input feature back as part of residual learning, ensuring the production of clear and high-quality de-rained images.

## IV. EXPERIMENTS

### A. Implementation Details

In our experiments, we configure the TransformerBlock with a head count of 2 and set the channel expansion factor in the GRDB to 2.66. The number of channels in the intermediate layers of our architecture is established at 128. In the training phase, we employ the Adam optimizer, starting with momentum values of 0.9 and 0.999. The initial learning rate is set at 0.0001, and we adopt a cyclic strategy

for adjusting the learning rate, with a peak set at 0.0003. Our models are trained on  $256 \times 256$  patches with batch sizes of 64 for approximately 800,000 iterations. Additionally, we implement a data augmentation strategy involving horizontal and vertical flips during training. Experiments are performed using the PyTorch framework on eight NVIDIA GeForce RTX 3090 GPUs.

### B. Metrics.

Following previous works [56], we employ the Peak Signal-to-Noise Ratio (PSNR) [60] and the Structure Similarity Index Measure (SSIM) [61] to quantitatively assess performance on the luminance (Y) channel of synthetic datasets. For evaluating the effectiveness of our deraining approach on real-world scenes, we utilize the Naturalness Image Quality Evaluator (NIQE) [62] and the Blind/Referenceless Image Spatial Quality Evaluator (BRISQUE) [63] for our assessments.. It is important to note that higher values of PSNR and SSIM signify improved performance, whereas lower scores for NIQE and BRISQUE are desirable.

### C. Comparisons with State-of-the-art Methods

To demonstrate the superiority of our method, we compare our model with twenty-four existing state-of-the-art deraining methods on two prevailing deraining benchmarks, including GMM [4], DerainNet [41], JCAS [54], DDN [41], SEMI [49], DIDMDN [42], UMRL [35], RESCAN [36], NLEDN [55], SPANet [50], PReNet [37], JORDER-E [56], MSPFN [38], CRDNet [9], MPRNet [39], IDLIR [51], Uformer-B [52], CCN [57], IDT [44], Semi-SwinDerain [34], LDRNet [53], Uformer [52], NAFNet [58] and DGUNet [59].

### D. Datasets

**Synthetic Data.** Following in [39], we train our model on the widely-used Rain13K dataset, which comprises 13,712 clean-rain image pairs sourced from multiple synthetic datasets. These test sets include Rain100H [56], Test100 [64], Rain100L [56], Test2800 [41], and Test1200 [42].

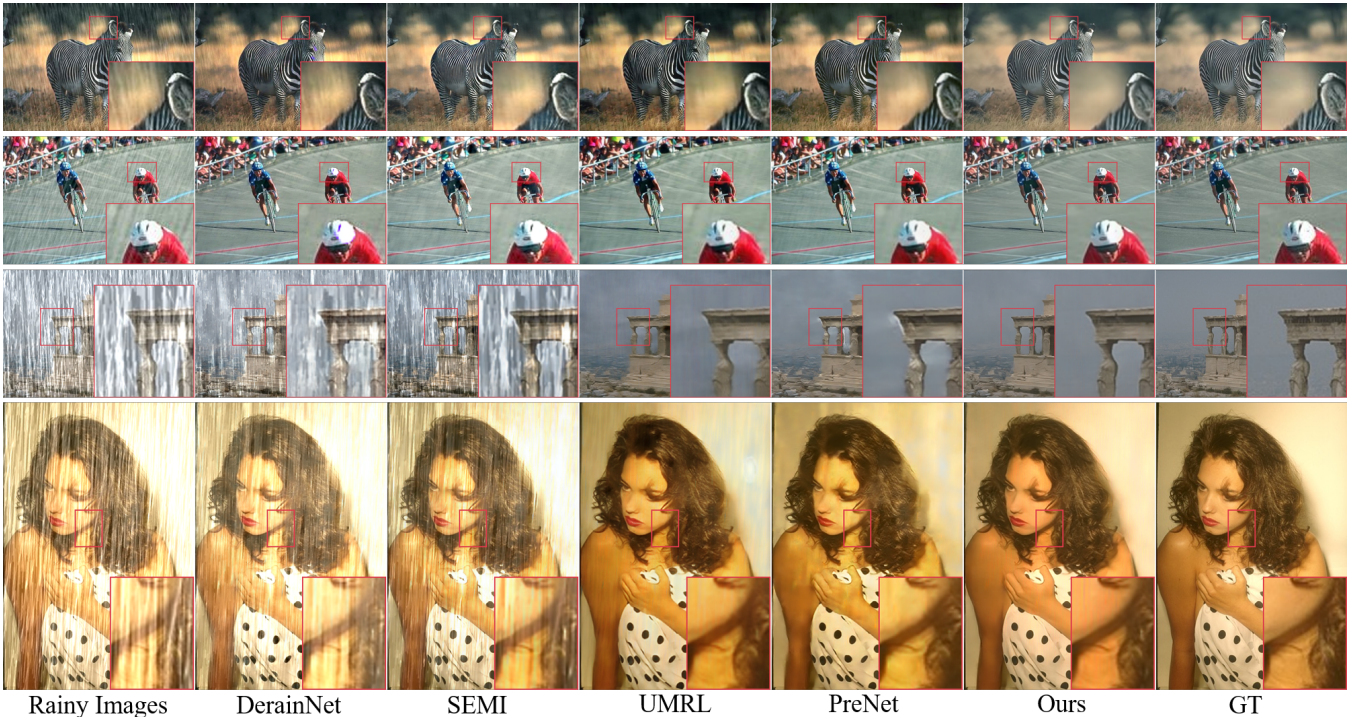


Fig. 5. Visual Comparison with Existing Deraining Methods on the Rain100H and Test100 Datasets. The highlighted red boxes focus on the detailed aspects of the deraining results. Please zoom in for an enhanced view.

TABLE III  
NIQE( $\downarrow$ )/BRISQUE( $\downarrow$ ) PERFORMANCE COMPARISONS ON THE  
REAL-WORLD DATASETS REAL15 AND REAL300.

Datasets	UMRL [35]	PreNet [37]	MSPFN [38]	MPRNet [39]	AFENet(Ours)
Real15	16.60/24.09	16.04/25.29	17.03/23.60	16.48/23.92	<b>15.90/23.18</b>
Real300	15.78/26.39	15.12/ <b>23.57</b>	15.34/28.27	15.08/28.69	<b>15.01/26.34</b>

Additionally, to verify the effectiveness of our method across different rain scenes, we employ the RainDS benchmark datasets [8] for both training and evaluation. The RainDS dataset, which includes image pairs with rain streaks (RS), raindrops (RD), and both (RDS), comprises 3600 pairs in total. Of these, 3000 are allocated for training purposes and the remaining 600 are utilized for testing.

**Real-world Data.** To assess the efficacy of our proposed method in real-world scenarios, we use the Real15 [56] and Real300 [65] datasets. These datasets, containing 15 and 300 rainy images captured from real-world rainy scenes, respectively, are employed to evaluate our methods and compare them with existing deraining approaches.

### E. Quantitative Analysis

To illustrate the superiority of our method, we conduct comparisons with twenty-four existing state-of-the-art deraining methods across two public benchmarks. The results, as presented in Table I and Table II, show that our method achieves the highest performance in terms of PSNR and SSIM. Notably, on the Rain13k benchmark, our method outperforms the previous state-of-the-art LDRNet by 0.23

dB in PSNR and 0.007 in SSIM. This indicates our method’s effectiveness in removing a variety of rain streaks and reconstructing more detailed imagery. Additionally, as Table II demonstrates, our method outperforms others on the RainDS benchmark, which includes both rain streaks and raindrops. Specifically, we exceed the performance of the leading deraining method, DGUNet [59], by 2.08 dB in PSNR for the RS scene and by 1.11 dB in PSNR for the RD scene. This highlights our method’s ability to effectively eliminate complex rainy degradation patterns and deliver superior deraining results.

We conduct comparisons with existing approaches under two publicly available real rainy scene conditions to further demonstrate the generalization capabilities of our proposed method. The results are presented in Table III. We observe that our method achieves the best performance on the no-reference metrics NIQE and BRISQUE in real-world scenarios. This demonstrates the generalizability of our approach in real-world scenarios and underscores the potential of the proposed method for deployment in practical environments.

### F. Qualitative Analysis

To showcase the visual superiority of our approach, we perform comparative analyses with existing deraining methods on Rain100H and Test100, as shown in Fig. 5. It is evident that our method more effectively removes rain streaks compared to others like SEMI and UMRL, which leave residual rain streaks in their deraining results. Our method particularly excels in detail restoration. Thanks to our innovative Frequency Enhancement Module (FEM) and

region-adaptive Frequency Aggregation Module (FAM), it not only removes rain streaks but also preserves reliable image details. This demonstrates our method’s consistent improvement across various frequency bands, underscoring its robustness and generalization capabilities in diverse rainy conditions.

TABLE IV  
STUDIES ON DIFFERENT SETTINGS

	S1	S2	S3	S4	Ours
PSNR	32.48	32.04	32.98	32.44	<b>33.27</b>
SSIM	0.919	0.912	0.929	0.917	<b>0.933</b>

### G. Ablation Study

To validate the effectiveness of each proposed component in our proposed method, we perform the following ablation studies: (S1): Without frequency decomposition module, we simply feed a full-frequency rainy image into the branch of the frequency enhancement module; (S2): The frequency decomposition module implemented using convolution is replaced with DCT for frequency decomposition; (S3): Without interaction between different frequency branches; (S4): Using concatenation to replace the frequency aggregation module. In Table IV, we can observe that all components are crucial for our AFENet. For example, comparing S1, S2, and our method, which demonstrates frequency separation using convolution for frequency separation is effective. The performance of the proposed method degrades by 0.29 dB and 0.004 on PSNR and SSIM without interaction, demonstrating the superiority of our frequency interaction strategy. The performance of the proposed method degrades 0.83 dB and 0.016 on PSNR and SSIM without aggregation, demonstrating that long-range dependencies from multi-scale feature representations can be used to identify and restore valuable features for clean image reconstruction more effectively.

### V. CONCLUSION

In this paper, we introduce an innovative end-to-end Adaptive Frequency Enhancement Network (AFENet), leveraging our uniquely designed Frequency Enhancement Module and Feature Aggregation Module. These modules work in tandem to accomplish feature enhancement and fusion across different frequency branches. AFENet demonstrates a remarkable ability to adaptively enhance features in various frequency components, thus effectively producing high-quality images that are free from rain artifacts. The proposed network is evaluated on four public deraining benchmarks, including both synthetic and real. Extensive experiments have consistently shown that AFENet not only excels beyond the current state-of-the-art deraining methods but also delivers visually impressive enhancement results.

### REFERENCES

[1] Wenhan Yang, Robby T Tan, Shiqi Wang, Yuming Fang, and Jiaying Liu, “Single image deraining: From model-based to data-driven and beyond,” *IEEE Transactions on pattern analysis and machine intelligence*, vol. 43, no. 11, pp. 4059–4077, 2020.

[2] Paolo Testolina, Francesco Barbato, Umberto Michieli, Marco Giordani, Pietro Zanuttigh, and Michele Zorzi, “Selma: Semantic large-scale multimodal acquisitions in variable weather, daytime and viewpoints,” *IEEE Transactions on Intelligent Transportation Systems*, 2023.

[3] Long Peng, Yang Cao, Yuejin Sun, and Yang Wang, “Lightweight adaptive feature de-drifting for compressed image classification,” *IEEE Transactions on Multimedia*, pp. 1–13, 2024.

[4] Yu Li, Robby T Tan, Xiaojie Guo, Jiangbo Lu, and Michael S Brown, “Rain streak removal using layer priors,” in *Proceedings of the IEEE conference on computer vision and pattern recognition*, 2016, pp. 2736–2744.

[5] Lei Zhu, Chi-Wing Fu, Dani Lischinski, and Pheng-Ann Heng, “Joint bi-layer optimization for single-image rain streak removal,” in *Proceedings of the IEEE international conference on computer vision*, 2017, pp. 2526–2534.

[6] Yinglong Wang, Shuaicheng Liu, Chen Chen, and Bing Zeng, “A hierarchical approach for rain or snow removing in a single color image,” *IEEE Transactions on Image Processing*, vol. 26, no. 8, pp. 3936–3950, 2017.

[7] Sixiang Chen, Tian Ye, Yun Liu, Erkang Chen, Jun Shi, and Jingchun Zhou, “Snowformer: Scale-aware transformer via context interaction for single image desnowing,” *arXiv preprint arXiv:2208.09703*, 2022.

[8] Sixiang Chen, Tian Ye, Jinbin Bai, Erkang Chen, Jun Shi, and Lei Zhu, “Sparse sampling transformer with uncertainty-driven ranking for unified removal of raindrops and rain streaks,” in *Proceedings of the IEEE/CVF International Conference on Computer Vision*, 2023, pp. 13106–13117.

[9] Long Peng, Aiwon Jiang, Qiaosi Yi, and Mingwen Wang, “Cumulative rain density sensing network for single image derain,” *IEEE Signal Processing Letters*, vol. 27, pp. 406–410, 2020.

[10] Deniz Engin, Anil Genç, and Hazim Kemal Ekenel, “Cycle-dehaze: Enhanced cyclegan for single image dehazing,” in *Proceedings of the IEEE conference on computer vision and pattern recognition workshops*, 2018, pp. 825–833.

[11] Kaihao Zhang, Wenhan Luo, Yiran Zhong, Lin Ma, Bjorn Stenger, Wei Liu, and Hongdong Li, “Deblurring by realistic blurring,” in *Proceedings of the IEEE/CVF Conference on Computer Vision and Pattern Recognition*, 2020, pp. 2737–2746.

[12] Codruta O Ancuti, Cosmin Ancuti, Florin-Alexandru Vasluiianu, and Radu Timofte, “Ntire 2020 challenge on nonhomogeneous dehazing,” in *Proceedings of the IEEE/CVF Conference on Computer Vision and Pattern Recognition Workshops*, 2020, pp. 490–491.

[13] Qiuhai Yan, Aiwon Jiang, Kang Chen, Long Peng, Qiaosi Yi, and Chunjie Zhang, “Textual prompt guided image restoration,” *arXiv preprint arXiv:2312.06162*, 2023.

[14] Yawei Li, Yulun Zhang, Radu Timofte, Luc Van Gool, Lei Yu, Youwei Li, Xinpeng Li, Ting Jiang, Qi Wu, Mingyan Han, et al., “Ntire 2023 challenge on efficient super-resolution: Methods and results,” in *Proceedings of the IEEE/CVF Conference on Computer Vision and Pattern Recognition*, 2023, pp. 1921–1959.

[15] Yuhong He, Tao Zeng, Ye Xiong, Jialu Li, and Haoran Wei, “Deep leaning based frequency-aware single image deraining by extracting knowledge from rain and background,” *Machine Learning and Knowledge Extraction*, vol. 4, no. 3, pp. 738–752, 2022.

[16] Siyuan Li, Wenqi Ren, Feng Wang, Iago Breno Araujo, Eric K Tokuda, Roberto Hirata Junior, Roberto M Cesar-Jr, Zhangyang Wang, and Xiaochun Cao, “A comprehensive benchmark analysis of single image deraining: Current challenges and future perspectives,” *International Journal of Computer Vision*, vol. 129, pp. 1301–1322, 2021.

[17] Zhipeng Su, Yixiong Zhang, Jianghong Shi, and Xiao-Ping Zhang, “A survey of single image rain removal based on deep learning,” *ACM Computing Surveys*, vol. 56, no. 4, pp. 1–35, 2023.

[18] Long Peng, Aiwon Jiang, Haoran Wei, Bo Liu, and Mingwen Wang, “Ensemble single image deraining network via progressive structural boosting constraints,” *Signal Processing: Image Communication*, vol. 99, pp. 116460, 2021.

[19] Zhifeng Wang, Aiwon Jiang, Chunjie Zhang, Hanxi Li, and Bo Liu, “Self-supervised multi-scale pyramid fusion networks for realistic bokeh effect rendering,” *Journal of Visual Communication and Image Representation*, vol. 87, pp. 103580, 2022.

[20] Zhifeng Wang and Aiwon Jiang, “A dense prediction vit network for single image bokeh rendering,” in *Chinese Conference on Pattern Recognition and Computer Vision (PRCV)*. Springer, 2022, pp. 213–222.

- [21] Yang Wang, Long Peng, Liang Li, Yang Cao, and Zheng-Jun Zha, "Decoupling-and-aggregating for image exposure correction," in *Proceedings of the IEEE/CVF Conference on Computer Vision and Pattern Recognition*, 2023, pp. 18115–18124.
- [22] Long Peng, Yang Cao, Yuejin Sun, and Yang Wang, "Lightweight adaptive feature de-drifting for compressed image classification," *IEEE Transactions on Multimedia*, 2024.
- [23] Long Peng, Wenbo Li, Renjing Pei, Jingjing Ren, Yang Wang, Yang Cao, and Zheng-Jun Zha, "Towards realistic data generation for real-world super-resolution," *arXiv preprint arXiv:2406.07255*, 2024.
- [24] Long Peng, Yang Cao, Renjing Pei, Wenbo Li, Jiaming Guo, Xueyang Fu, Yang Wang, and Zheng-Jun Zha, "Efficient real-world image super-resolution via adaptive directional gradient convolution," *arXiv preprint arXiv:2405.07023*, 2024.
- [25] Yuhong He, Long Peng, Lu Wang, and Jun Cheng, "Latent degradation representation constraint for single image deraining," in *ICASSP 2024-2024 IEEE International Conference on Acoustics, Speech and Signal Processing (ICASSP)*. IEEE, 2024, pp. 3155–3159.
- [26] Aiwen Jiang, Zhi Wei, Long Peng, Feiqiang Liu, Wenbo Li, and Mingwen Wang, "Dalpr: Leverage degradation-aligned language prompt for real-world image super-resolution," *arXiv preprint arXiv:2406.16477*, 2024.
- [27] Chen Wu, Zhuoran Zheng, Xiuyi Jia, and Wenqi Ren, "Mixnet: Towards effective and efficient uhd low-light image enhancement," *arXiv preprint arXiv:2401.10666*, 2024.
- [28] Jie Zhang, Xiaohua Qi, and Bo Zhao, "Federated generative learning with foundation models," *arXiv preprint arXiv:2306.16064*, 2023.
- [29] Qiaosi Yi, Faming Fang, Guixu Zhang, and Tiejong Zeng, "Frequency learning via multi-scale fourier transformer for mri reconstruction," *IEEE Journal of Biomedical and Health Informatics*, 2023.
- [30] Qiaosi Yi, Juncheng Li, Qinyan Dai, Faming Fang, Guixu Zhang, and Tiejong Zeng, "Structure-preserving deraining with residue channel prior guidance," in *Proceedings of the IEEE/CVF international conference on computer vision*, 2021, pp. 4238–4247.
- [31] Qiaosi Yi, Juncheng Li, Faming Fang, Aiwen Jiang, and Guixu Zhang, "Efficient and accurate multi-scale topological network for single image dehazing," *IEEE Transactions on Multimedia*, vol. 24, pp. 3114–3128, 2021.
- [32] Haodian Wang, Long Peng, Yuejin Sun, Zengyu Wan, Yang Wang, and Yang Cao, "Brightness perceiving for recursive low-light image enhancement," *IEEE Transactions on Artificial Intelligence*, 2023.
- [33] Yu Luo, Yong Xu, and Hui Ji, "Removing rain from a single image via discriminative sparse coding," in *Proceedings of the IEEE international conference on computer vision*, 2015, pp. 3397–3405.
- [34] Chun Ren, Danfeng Yan, Yuanqiang Cai, and Yangchun Li, "Semi-swinderain: Semi-supervised image deraining network using swin transformer," in *ICASSP 2023-2023 IEEE International Conference on Acoustics, Speech and Signal Processing (ICASSP)*. IEEE, 2023, pp. 1–5.
- [35] Rajeev Yasarla and Vishal M Patel, "Uncertainty guided multi-scale residual learning-using a cycle spinning cnn for single image deraining," in *Proceedings of the IEEE/CVF conference on computer vision and pattern recognition*, 2019, pp. 8405–8414.
- [36] Xia Li, Jianlong Wu, Zhouchen Lin, Hong Liu, and Hongbin Zha, "Recurrent squeeze-and-excitation context aggregation net for single image deraining," in *Proceedings of the European conference on computer vision (ECCV)*, 2018, pp. 254–269.
- [37] Dongwei Ren, Wangmeng Zuo, Qinghua Hu, Pengfei Zhu, and Deyu Meng, "Progressive image deraining networks: A better and simpler baseline," in *Proceedings of the IEEE conference on computer vision and pattern recognition*, 2019, pp. 3937–3946.
- [38] Kui Jiang, Zhongyuan Wang, Peng Yi, Chen Chen, Baojin Huang, Yimin Luo, Jiayi Ma, and Junjun Jiang, "Multi-scale progressive fusion network for single image deraining," in *Proceedings of the IEEE/CVF conference on computer vision and pattern recognition*, 2020, pp. 8346–8355.
- [39] Syed Waqas Zamir, Aditya Arora, Salman Khan, Munawar Hayat, Fahad Shahbaz Khan, Ming-Hsuan Yang, and Ling Shao, "Multi-stage progressive image restoration," in *Proceedings of the IEEE/CVF conference on computer vision and pattern recognition*, 2021, pp. 14821–14831.
- [40] Yang Wang, Jing Zhang, Yang Cao, and Zengfu Wang, "A deep cnn method for underwater image enhancement," in *2017 IEEE international conference on image processing (ICIP)*. IEEE, 2017, pp. 1382–1386.
- [41] Xueyang Fu, Jiabin Huang, Delu Zeng, Yue Huang, Xinghao Ding, and John Paisley, "Removing rain from single images via a deep detail network," in *Proceedings of the IEEE conference on computer vision and pattern recognition*, 2017, pp. 3855–3863.
- [42] He Zhang and Vishal M Patel, "Density-aware single image de-raining using a multi-stream dense network," in *Proceedings of the IEEE conference on computer vision and pattern recognition*, 2018, pp. 695–704.
- [43] Yuntong Ye, Yi Chang, Hanyu Zhou, and Luxin Yan, "Closing the loop: Joint rain generation and removal via disentangled image translation," in *Proceedings of the IEEE/CVF conference on computer vision and pattern recognition*, 2021, pp. 2053–2062.
- [44] Jie Xiao, Xueyang Fu, Aiping Liu, Feng Wu, and Zheng-Jun Zha, "Image de-raining transformer," *IEEE Transactions on Pattern Analysis and Machine Intelligence*, 2022.
- [45] Yanni Zhang, Qiang Li, Miao Qi, Di Liu, Jun Kong, and Jianzhong Wang, "Multi-scale frequency separation network for image deblurring," *IEEE Transactions on Circuits and Systems for Video Technology*, 2023.
- [46] Tomohiko Nakamura and Hiroshi Saruwatari, "Time-domain audio source separation based on wave-u-net combined with discrete wavelet transform," in *ICASSP 2020-2020 IEEE International Conference on Acoustics, Speech and Signal Processing (ICASSP)*. IEEE, 2020, pp. 386–390.
- [47] Zizheng Pan, Jianfei Cai, and Bohan Zhuang, "Fast vision transformers with hilo attention," *Advances in Neural Information Processing Systems*, vol. 35, pp. 14541–14554, 2022.
- [48] Syed Waqas Zamir, Aditya Arora, Salman Khan, Munawar Hayat, Fahad Shahbaz Khan, and Ming-Hsuan Yang, "Restormer: Efficient transformer for high-resolution image restoration," in *Proceedings of the IEEE/CVF conference on computer vision and pattern recognition*, 2022, pp. 5728–5739.
- [49] Wei Wei, Deyu Meng, Qian Zhao, Zongben Xu, and Ying Wu, "Semi-supervised transfer learning for image rain removal," in *Proceedings of the IEEE/CVF conference on computer vision and pattern recognition*, 2019, pp. 3877–3886.
- [50] Tianyu Wang, Xin Yang, Ke Xu, Shaozhe Chen, Qiang Zhang, and Rynson WH Lau, "Spatial attentive single-image deraining with a high quality real rain dataset," in *Proceedings of the IEEE/CVF Conference on Computer Vision and Pattern Recognition*, 2019, pp. 12270–12279.
- [51] Mingyu Ma, Dongwei Ren, and Yajun Yang, "Integrating degradation learning into image restoration," in *2022 IEEE International Conference on Multimedia and Expo (ICME)*. IEEE, 2022, pp. 1–6.
- [52] Zhendong Wang, Xiaodong Cun, Jianmin Bao, Wengang Zhou, Jianzhuang Liu, and Houqiang Li, "Uformer: A general u-shaped transformer for image restoration," in *Proceedings of the IEEE/CVF conference on computer vision and pattern recognition*, 2022, pp. 17683–17693.
- [53] Yuhong He, Long Peng, Lu Wang, and Jun Cheng, "Latent degradation representation constraint for single image deraining," *arXiv preprint arXiv:2309.04780*, 2023.
- [54] Shuhang Gu, Deyu Meng, Wangmeng Zuo, and Lei Zhang, "Joint convolutional analysis and synthesis sparse representation for single image layer separation," in *Proceedings of the IEEE International Conference on Computer Vision*, 2017, pp. 1708–1716.
- [55] Guanbin Li, Xiang He, Wei Zhang, Huiyou Chang, Le Dong, and Liang Lin, "Non-locally enhanced encoder-decoder network for single image de-raining," in *Proceedings of the 26th ACM international conference on Multimedia*, 2018, pp. 1056–1064.
- [56] Wenhan Yang, Robby T Tan, Jiashi Feng, Jiaying Liu, Zongming Guo, and Shuicheng Yan, "Deep joint rain detection and removal from a single image," in *Proceedings of the IEEE conference on computer vision and pattern recognition*, 2017, pp. 1357–1366.
- [57] Ruijie Quan, Xin Yu, Yuanzhi Liang, and Yi Yang, "Removing raindrops and rain streaks in one go," in *Proceedings of the IEEE/CVF Conference on Computer Vision and Pattern Recognition*, 2021, pp. 9147–9156.
- [58] Liangyu Chen, Xiaojie Chu, Xiangyu Zhang, and Jian Sun, "Simple baselines for image restoration," in *European Conference on Computer Vision*. Springer, 2022, pp. 17–33.
- [59] Chong Mou, Qian Wang, and Jian Zhang, "Deep generalized unfolding networks for image restoration," in *Proceedings of the IEEE/CVF Conference on Computer Vision and Pattern Recognition*, 2022, pp. 17399–17410.



- [60] Quan Huynh-Thu and Mohammed Ghanbari, "Scope of validity of psnr in image/video quality assessment," *Electronics letters*, vol. 44, no. 13, pp. 800–801, 2008.
- [61] Zhou Wang, Alan C Bovik, Hamid R Sheikh, and Eero P Simoncelli, "Image quality assessment: from error visibility to structural similarity," *IEEE Transactions on Image Processing*, vol. 13, no. 4, pp. 600–612, 2004.
- [62] Anish Mittal, Rajiv Soundararajan, and Alan C Bovik, "Making a "completely blind" image quality analyzer," *IEEE Signal processing letters*, vol. 20, no. 3, pp. 209–212, 2012.
- [63] Anish Mittal, Anush K Moorthy, and Alan C Bovik, "Blind/referenceless image spatial quality evaluator," in *2011 conference record of the forty fifth asilomar conference on signals, systems and computers (ASILOMAR)*. IEEE, 2011, pp. 723–727.
- [64] He Zhang, Vishwanath Sindagi, and Vishal M Patel, "Image de-raining using a conditional generative adversarial network," *IEEE transactions on circuits and systems for video technology*, vol. 30, no. 11, pp. 3943–3956, 2019.
- [65] Xueyang Fu, Borong Liang, Yue Huang, Xinghao Ding, and John Paisley, "Lightweight pyramid networks for image deraining," *IEEE transactions on neural networks and learning systems*, vol. 31, no. 6, pp. 1794–1807, 2019.